International Journal of Heat and Mass Transfer 65 (2013) 855–862

Contents lists available at SciVerse ScienceDirect

International Journal of Heat and Mass Transfer

journal homepage: www.elsevier.com/locate/ijhmt

Mean flow effects in magneto-convection

Y. Rameshwar [a,*], M.A. Rawoof Sayeed [b], H.P. Rani [c], D. Laroze [d,e]

[a] Department of Mathematics, University College of Science, Osmania University, Saifabad, Hyderabad 500004, India
[b] Department of Mathematics, Muffakham Jah College of Engineering and Technology, Hyderabad 500034, India
[c] Department of Mathematics, National Institute of Technology, Warangal 506004, India
[d] Max Planck Institute for Polymer Research, D 55021 Mainz, Germany
[e] Instituto de Alta Investigación, Universidad de Tarapacá, Casilla 7D, Arica, Chile

ARTICLE INFO

Article history:
Received 18 January 2013
Received in revised form 3 May 2013
Accepted 18 June 2013
Available online 25 July 2013

Keywords:
Thermal convection
Electrically conducing fluid
Magnetic field

ABSTRACT

In the present study the theoretical and numerical results of Rayleigh-Bérnard convection in an electrically conducing fluid in the presence of a vertical external magnetic field is reported. The effect of mean flow at the onset of stationary convection and close to the bifurcation is analyzed. The coefficients of the corresponding amplitude equations are analytically calculated and numerical simulations are performed. Finally, the secondary instabilities, such as Eckhaus, zig-zag and skew-varicose at the onset of stationary convection, associated to the roll solution are studied. It is observed that most of the critical modes appear close to the zig-zag instability.

1. Introduction

Magneto-convection is the study of thermal convection within a conducting liquid under the influence of an external magnetic field. This type of study was primarily motivated by the geophysical and astrophysical applications, in particular, by the observation of sunspots in the imposed magnetic field conditions and by the magnetic fields on other planets [1–4].

In this context, it is important to understand how the Lorentz force affects the convective motion in many astrophysical and geophysical problems. Whenever thermal convection takes place in an electrically and thermally conducting fluid of planetary or stellar dimensions, it is always associated with the presence of magnetic fields. The presence of strong magnetic fields modifies the thermal convection of the outer layers of Sun and other late type stars. Another reason to study the influence of magnetic field on the thermal convection is that it produces a narrowing of convective rolls that suppresses the amplitude of convection and gives rise to a variety of patterns, which are typical to nonlinear systems.

Theoretical studies of convection within the framework of the Boussinesq approximation have been inspired mainly by the existence of sunspots. The linear problem at the onset of convection in the presence of homogenous magnetic field can be found in Refs. [5,6]. Similar experimental studies have been carried out by Nakagawa [7]. This application has motivated several other authors to investigate the suppression of convection and the occurrence of different patterns by strong magnetic fields [8–12].

More complicated convection patterns mix the transverse and the longitudinal modes, in contrast to zig-zag stripes that leads to a mean flow. This long wavelength instability generates skew-varicose instabilities. The instability of rolls specific to stress-free boundaries, which depend on the existence of a slowly decaying large scale mode in the absence of magnetic field and at the onset for Rayleigh–Benard model, were first studied by Zipplieus and Siggia [13,14]. The authors have obtained the sufficient conditions for the secondary instabilities such as Eckhaus, zig-zag, cross-roll and skew-varicose instabilities near the onset using the amplitude equations. The authors have shown that no stable rolls exist for a thermal Prandtl number (P_r) less than 0.728. Also, Busse and Bolton [15] obtained the marginal instability of rolls by the direct calculation of unstable mode and claimed that for $P_r < 0.543$, no stable rolls exist. This result was confirmed by Bernoff [16], who studied the instability of the rolls using the Ginzburg–Landau equation. Milke [17] showed that the difference in stability thresholds with those of Zipplieus and Siggia [14] and Busse and Bolton [15], is due to the difference in the assumption of asymptotic relations between the parameters that characterize the problem, and hence corresponds to two different unstable modes. Podivigina [18] studied the stability of the rolls without these prior assumptions and claimed that a new stability threshold also exist for $0.543 < P_r < 0.782$.

In recent years, several authors have discussed the possibility that slowly varying long-wavelength quantities can significantly affect the convective cells by changing their stability properties

* Corresponding author. Tel.: +91 8977241872.
E-mail addresses: yrhwrr1@yahoo.co.in, hprani@nitw.ac.in (Y. Rameshwar).

0017-9310/$ - see front matter © 2013 Elsevier Ltd. All rights reserved.
http://dx.doi.org/10.1016/j.ijheatmasstransfer.2013.06.041

Nomenclature

A	amplitude
B_x	the contribution of mean flow generated by a vertical vorticity component
C_z	the contribution of mean flow generated by a vertical magnetic current component
d	depth of the convection zone
$\mathbf{g}$	gravitational field
$\mathbf{H}$	external magnetic field
$\mathbf{H}_0$	external magnetic field along z-axis
H_x, H_y, H_z	components of magnetic field
$\mathbf{J}$	current
k	wave number
k_{sc}	critical wave number
$\mathcal{L}$	linear operator
$\mathcal{N}$	nonlinear operator
p_{eff}	effective pressure
P_m	magnetic Prandtl number
P_r	thermal Prandtl number
q_X, q_Y	wave numbers along X, Y direction
Q	Chandrasekar Number
Ra	Rayleigh number
Ra_s	stationary Rayleigh number
Ra_{sc}	critical Rayleigh number
T	slow time scale
t	time coordinate
$\mathbf{v}$	velocity
v_x, v_y, v_z	velocity components
x, y, z	cartesian coordinates
X, Y	horizontal and vertical spatial scales
NWS	Newell-Whitehead-Segel

Greek symbols

τ	temperature
$\Delta\tau$	temperature difference between upper and lower layers
θ	perturbed temperature
β	adverse temperature gradient
ρ_0	reference mass density
κ	coefficients of thermal diffusivity
ν	viscosity
η	magnetic diffusivity
α	coefficients of thermal expansion
μ_m	magnetic permeability
ω	vorticity

Superscript

$'$	variables with dimension

at the onset [19–22]. Cox and Matthews [23] showed that the inclusion of large scale modes of magnetic flux is essential to obtain correct determination of stability of convective rolls. They have derived an amplitude equation for magneto-convection and anticipated that this model will have application for a wide range of pattern formation problems. Furthermore, they suggested that their nonlinear analysis for convection under the influence of magnetic field confines to a stationary bifurcation. Using their amplitude equation, they have also shown the regions, where the rolls become unstable, stable and subcritical. They have obtained the conditions of instability for new convective rolls under the influence of magnetic field and discussed that this new instability of convective rolls is quite different from that of the Eckhaus instability (a phase instability). This new type of instability is amplitude driven, leading to a stable pattern of rolls in which the amplitude changes on long spatial scales. Other important works about the magneto-convection can be found in Refs. [24–30].

In the present study the problem of nonlinear magneto-convection in the presence of a magnetic field along with the Boussinesq approximation for idealized boundary conditions is analyzed. Following the Zipplieus and Siggia [14] approach a set of amplitude equations were derived by taking into account of the mean flow effects. The corresponding secondary instabilities such as Eckhaus, zig-zag and skew-varicose at the onset of stationary convection are studied. The paper is organized as follows: In Section 2, the basic hydrodynamic equations are presented. In Section 3, a set of two dimensional amplitude equations at the onset of stationary convection is derived and some numerical simulations are performed. In Section 4 the secondary instabilities are analyzed. Finally, the conclusions are presented in Section 5.

2. Theoretical model

A layer of incompressible electrically and thermally conducting fluid, of thickness d, parallel to the xy-plane, with large horizontal extension in a gravitational field $\mathbf{g}$ and subjected to a vertical temperature gradient is considered. The external magnetic field $\mathbf{H}_0$ is assumed to be oriented in a direction parallel to the $\hat{\mathbf{z}}$ axis. The z-axis is chosen such that $\mathbf{g} = -g\hat{\mathbf{z}}$ and the layer has its interfaces at the coordinates $z = 0$ and d. A static temperature difference across the layer is imposed i.e.,$\tau(z = 0) = \tau_0 + \triangle\tau$ and $\tau(z = d) = \tau_0$. Under the Boussinesq approximation, the dimensionless equations for the perturbations of the conductive rest state can be written as [5]

$$\nabla \cdot \mathbf{v} = 0, \tag{1}$$

$$\frac{1}{P_r} d_t \mathbf{v} - \frac{QP_m}{P_r}(\mathbf{H} \cdot \nabla)\mathbf{H} = -\nabla p_{eff} + \nabla^2 \mathbf{v} + Q\frac{\partial \mathbf{H}}{\partial z} + Ra\theta\hat{\mathbf{z}}, \tag{2}$$

$$d_t\theta = \nabla^2\theta + v_z, \tag{3}$$

$$\frac{P_m}{P_r}\frac{\partial \mathbf{H}}{\partial t} = \nabla^2\mathbf{H} + \nabla \times (\mathbf{v} \times \hat{\mathbf{z}}) + \frac{P_m}{P_r}\nabla \times \mathbf{v} \times \mathbf{H}, \tag{4}$$

$$\nabla \cdot \mathbf{H} = 0, \tag{5}$$

where $\mathbf{v} = (v_x, v_y, v_z)^T$ denotes the fluid velocity perturbation, $\mathbf{H} = (H_x, H_y, H_z)^T$ is the magnetic field perturbation and θ is the perturbed temperature. In Appendix A, we have given the details of the occurrence of perturbed, dimensionless Eqs. (1)–(5) from the basic governing equations. Here the time derivative $d_t f (= \partial_t f + \mathbf{v} \cdot \nabla f)$ indicates the total derivative and p_{eff} is the effective pressure which contains both the hydrodynamic and the magnetic contributions. In Eqs. (1)–(5), the following groups of dimensionless numbers have been introduced: (a) (pure fluids) The Rayleigh number, $Ra = \alpha g \triangle\tau d^3/\kappa\nu$, accounting for the buoyancy effects and the thermal Prandtl number, $P_r = \nu/\kappa$, relates the viscous and thermal diffusion time scales. (b) (magnetic fluids) The magnetic Prandtl number $P_m = \nu/\eta$ measuring the ratio of magnetic to thermal diffusivity and the Chandrasekhar number is $Q = \mu_m H_0^2 d^2/4\pi\rho_0\nu\eta$. In these dimensionless numbers the different physical quantities represent α as the thermal expansion coefficient, κ the thermal diffusivity, ν the viscosity, η the magnetic diffusivity, μ_m the magnetic permeability and ρ_0 the reference mass density. With these non-dimensional

quantities, the effective pressure is given by $p_{eff} = (p + Q(P_r H_z + P_m |H|^2/2))/P_r$.

In the present analysis the following numerical values for the parameters were considered: the Ra can be usually changed by several orders of magnitude by varying the applied temperature gradient and in the present study, $Ra \sim 10^2$–10^3. A typical value for P_r in fluids is $P_r \sim 10^{-1}$–10^3 and in the earth mantle it is around 10^{25} [31]. The P_m can be relatively small in liquid metals of laboratory experiments [32] or very large ($P_m \gg 1$) in case of astrophysical situations [33] and in liquid metal laboratory dynamos. Similar to the Ra, the values of Q can be changed by several orders of magnitude by varying the applied magnetic field.

The following balance equation of the linear momentum without the effective pressure term is written by taking the curl operator twice on the Eq. (2) and combining it with the Eq. (1).

$$\left(\frac{1}{P_r}\frac{\partial}{\partial t} - \nabla^2\right)\nabla^2 \mathbf{v} = Q\nabla^2 \frac{\partial \mathbf{H}}{\partial z} + Ra\left(\nabla^2 \theta \hat{\mathbf{z}} - \nabla \frac{\partial \theta}{\partial z}\right) + \frac{1}{P_r}\nabla \times \mathbf{\Pi}(\mathbf{v}, \omega) - \frac{QP_m}{P_r}\nabla \times \mathbf{\Pi}(\mathbf{H}, \mathbf{J}), \tag{6}$$

where $\omega = \nabla \times \mathbf{v}$ denotes the vorticity, $\mathbf{J} = \nabla \times \mathbf{H}$ is the current and $\mathbf{\Pi}(\mathbf{a},\mathbf{b}) = (\mathbf{a}\cdot\nabla)\mathbf{b} - (\mathbf{b}\cdot\nabla)\mathbf{a}$.

Eqs. (3)–(6) can be written in a compact form as

$$\mathcal{L}\mathbf{u} + \mathcal{N}(\mathbf{u}|\mathbf{u}) = 0, \tag{7}$$

in which $\mathbf{u} = (v_x, v_y, v_z, H_x, H_y, H_z, \theta)^T$ and $\mathcal{L}$ and $\mathcal{N}$ stand for the linear and the nonlinear operators of the corresponding equations, respectively.

The idealized boundary conditions were imposed on both the boundaries, $z = 0$ and 1 [5]. Hence, the boundaries are stress free, maintained at a fixed temperature and a vertical magnetic field is imposed on the boundaries as

$$\frac{\partial v_x}{\partial z} = \frac{\partial v_y}{\partial z} = v_z = H_x = H_y = \theta = 0. \tag{8}$$

Also, the periodic boundary conditions are assumed along the horizontal directions. These conditions implies that the z-dependence is entirely given in terms of the trigonometric functions. In the next section, a weakly nonlinear analysis of the system (7) in the case of a stationary bifurcation is presented.

3. Effects of mean flow at the onset of stationary convection

As the linear instability at the threshold of the conducting state had been studied by many authors in different situations, only the main results of the linear analysis for the stationary case [5,6] are presented here. The stationary Ra obtained from the eigenvalue of the linear part of system (7) and is given by [5]:

$$Ra_s = \frac{\zeta^2(\zeta^4 + Q\pi^2)}{k^2}, \tag{9}$$

where $\zeta^2 = k^2 + n\pi^2$ is the augmented dimensionless wavenumber and in the present study $n = 1$ is considered. The minimum of the marginal curve ($\partial_k Ra_s = 0$) gives the critical wavenumber k_{sc} and the associated critical Rayleigh number, Ra_{sc}. The explicit expression of Ra_{sc} is [28]

$$Ra_{sc} = \frac{9\pi^4}{4}\left(\Lambda + 1 + \frac{1}{\Lambda}\right) + \pi^2 Q\left(1 + \frac{2}{\Lambda}\right), \tag{10}$$

where

$$\Lambda^3 = 1 + \frac{4Q}{3\pi^3} + \frac{8Q^2}{27\pi^4}\left(1 + \sqrt{1 + \frac{\pi^2}{Q}}\right).$$

Moreover, the k_{sc}, can be calculated from the Ra_{sc} as

$$k_{sc}^2 = \left(\frac{\pi^2 Ra_{sc}}{2}\right)^{\frac{1}{3}} - \pi^2 \tag{11}$$

It is observed that the threshold value increases when Q increases. Thus it can be inferred that the magnetic field has a stabilizing effect on the convective threshold. In addition from Eq. (9) it can be observed that the stationary threshold value is independent of both Prandtl numbers.

The control parameter, Ra_s is close to its threshold value Ra_{sc} if the bifurcation parameter is $\epsilon^2 = (Ra_s - Ra_{sc})/Ra_{sc}$. All functions were expanded in terms of ϵ and it is assumed that all variations of the linearized solutions were incorporated in the amplitude function, A and the fields, B_x and C_z. If these amplitudes are of size ϵ (i.e. $O(\epsilon)$) then the interaction of the convective cell with itself forces a second harmonic and a mean state of correction of size $O(\epsilon^{3/2})$, which in turn drives an $O(\epsilon^2)$ correction to the fundamental component of the imposed roll, and so on. A solvability criterion for the last correction yields a set of equations for $\{A(X,Y,T), B_x(X,Y,T), C_z(X,Y,T)\}$ of the imposed disturbances [14]. Therefore,

$$\mathbf{u} \to \epsilon(\mathbf{u}_0 + \epsilon^{1/2}\mathbf{u}_{3/2} + \epsilon\mathbf{u}_2 + \epsilon^{3/2}\mathbf{u}_{5/2} + \Theta(\epsilon^{5/2})) \tag{12}$$

and consequently $\mathcal{L} \to \mathcal{L}_0 + \epsilon^{1/2}\mathcal{L}_{3/2} + \epsilon\mathcal{L}_2 + \epsilon^{3/2}\mathcal{L}_{5/2} + \Theta(\epsilon^{5/2})$ and $\mathcal{N} \to \epsilon^{3/2}\mathcal{N}_0 + \epsilon^2\mathcal{N}_{3/2} + \epsilon^{5/2}\mathcal{N}_2 + \Theta(\epsilon^{7/2})$ where the expansions in the derivatives represent $\partial_x \to \partial_x + \epsilon\partial_X$, $\partial_y \to \partial_y + \epsilon^{1/2}\partial_Y$ and $\partial_t \to \partial_t + \epsilon^2\partial_T$, because A is a function of the slow time scale $T = \epsilon^2 t$ and the slow spatial scales $X = \epsilon x$ and $Y = \epsilon^{1/2} y$. Inserting these expansions in Eq. (7), for each power of ϵ, a hierarchy of equations was obtained by and is given by

$$\mathcal{L}_0\mathbf{u}_0 = 0, \tag{13}$$

$$\mathcal{L}_0\mathbf{u}_{3/2} = \mathcal{N}_0 - \mathcal{L}_{3/2}\mathbf{u}_0, \tag{14}$$

$$\mathcal{L}_0\mathbf{u}_2 = \mathcal{N}_{3/2} - \mathcal{L}_2\mathbf{u}_0 - \mathcal{L}_{3/2}\mathbf{u}_{3/2}, \tag{15}$$

$$\mathcal{L}_0\mathbf{u}_{5/2} = \mathcal{N}_2 - \mathcal{L}_{5/2}\mathbf{u}_0 - \mathcal{L}_2\mathbf{u}_{3/2} - \mathcal{L}_{3/2}\mathbf{u}_2. \tag{16}$$

These relationships were solved subsequently by fulfilling the solvability condition at each order. The following general non-linear equation was considered for further analysis.

$$\langle \mathbf{u}_0^\dagger | r.h.s. \rangle = \mathbf{0}, \tag{17}$$

where $\mathbf{u}_0^\dagger$ denotes the solution of the linear adjoint problem ($\mathcal{L}^+\mathbf{u}^\dagger = 0$). The notation $r.h.s$ corresponds to right hand side term of the perturbation and $\langle \circ \rangle$ denotes the inner product which is defined as a suitable volume integration. The solvability condition at $O(\epsilon^{5/2})$ leads to a set of equations for $\{A, B_x, C_z\}$ and are given by

$$\frac{\partial A}{\partial T} = A + \left(\frac{\partial}{\partial X} - i\frac{\partial^2}{\partial Y^2}\right)^2 A - |A|^2 A - iAB_x - \lambda_5 AC_z, \tag{18}$$

$$\gamma_1 \frac{\partial \omega_z}{\partial T} = \left(\frac{\partial^2}{\partial Y^2} + \delta\frac{\partial^2}{\partial X^2}\right)\omega_z + g_1\frac{\partial}{\partial Y}\left[A^*\left(\frac{\partial}{\partial X} - i\frac{\partial^2}{\partial Y^2}\right)A + c.c.\right], \tag{19}$$

$$\frac{\partial \omega_z}{\partial Y} = -\left(\frac{\partial^2}{\partial Y^2} + \delta\frac{\partial^2}{\partial X^2}\right)B_x, \tag{20}$$

$$\gamma_2 \frac{\partial J_x}{\partial T} = \left(\frac{\partial^2}{\partial Y^2} + \delta\frac{\partial^2}{\partial X^2}\right)J_x + g_2\left[\left(\frac{\partial^2}{\partial Y^2} + \delta\frac{\partial^2}{\partial X^2}\right)\left(A^*\frac{\partial A}{\partial Y} + c.c.\right)\right], \tag{21}$$

$$\frac{\partial J_x}{\partial Y} = \lambda_5\left(\frac{\partial^2}{\partial Y^2} + \delta\frac{\partial^2}{\partial X^2}\right)C_z, \tag{22}$$

where $\gamma_1 = \sqrt{\lambda_1\lambda_2}/(P_r k_{sc}\lambda_0)$, $\delta = \sqrt{\lambda_2\epsilon}/(4k_{sc}\sqrt{\lambda_1})$, $g_1 = \lambda_4\lambda_6/(P_r\lambda_3)$, $\gamma_2 = \gamma_1 P_m\sqrt{\epsilon}$ and $g_2 = \epsilon^2 P_m\lambda_2^2\lambda_7/(P_r\lambda_3\lambda_5)$. The explicit expressions

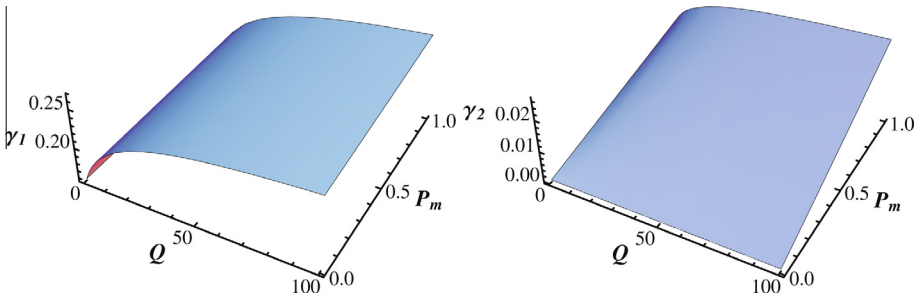

Fig. 1. Coefficients γ_1 (left) and γ_2 (right) as a function of Q and P_m for $P_r = 10$ and $\epsilon = 0.01$

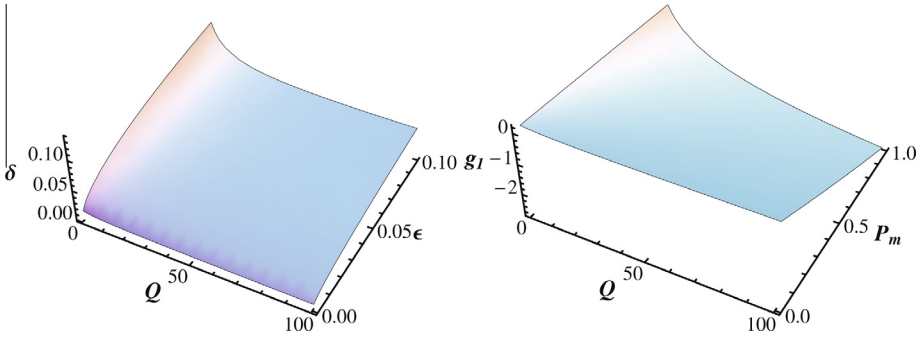

Fig. 2. For $P_r = 10$ the coefficient δ (left) as a function of Q and ϵ; and coefficient g_1 (right) as a function of Q and P_m.

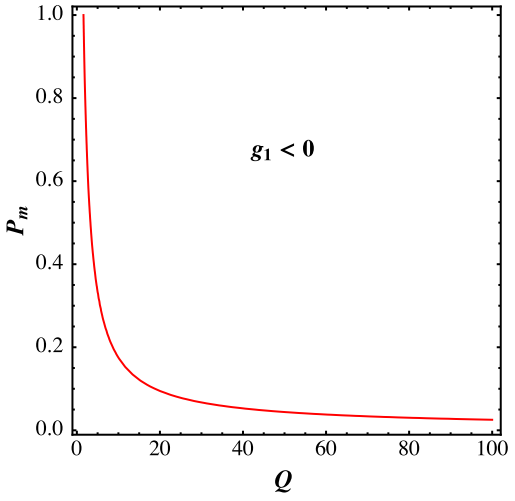

Fig. 3. Phase diagram of $g_1 = 0$ as a function of Q and P_m for $P_r = 10$.

for the coefficients λ_j, $j = 0$ to 7, are given in the Appendix B, nevertheless $\lambda_5 \propto Q$.

The shape of the coefficients, γ_1, γ_2, δ and g_1 that appear in the amplitude Eqs. (18)–(22) is analyzed with the aid of Figs. 1 and 2. Fig. 1 shows the dependence of Q and P_m on γ_1 and γ_2 coefficients. It can be observed that these coefficients are small in a wide range of parameters and increase when Q and P_m increase. For $P_r = 10$, the coefficients δ and g_1 are plotted in 2. From Fig. 2 it can be observed that the coefficient δ remained small for all range of both parameters Q and ϵ and this coefficient increases when ϵ increases while it decreases when Q increases. Also Fig. 2 shows when Q increases, the coefficient g_1 decreases and changes its sign. Fig. 3 show the phase diagram of Q and P_m when g_1 becomes zero and $P_r = 10$. From this figure it can be observed that P_m decays almost exponentially as a function of Q.

The set of Eqs. (18)–(22) have complex dynamical behaviors, as is shown in Fig. 4. In this figure we can observe multiple patterns transition, which continues changing dynamically. We solve numerically Eqs. (18)–(22) using the fourth order Runge–Kutta method with $\Delta T = 0.001$. A standard pseudo-spectral method was employed for the spatial discretization. Also, we impose periodic boundary conditions. The calculations were carried out in *Mathematica 8*. The initial conditions $A_r = B_x = C_z = 0$ and $A_i = -0.1$ were employed.

It can be noted that in the absence of magnetic field ($Q \to 0$), $\lambda_5 \to 0$. Then, the Eqs. (18)–(22) are reduced to

$$\frac{\partial A}{\partial T} = A + \left(\frac{\partial}{\partial X} - i\frac{\partial^2}{\partial Y^2}\right)^2 A - |A|^2 A - iAB_x, \tag{23}$$

$$\tilde{\gamma}_1 \frac{\partial \omega_z}{\partial T} = \left(\frac{\partial^2}{\partial Y^2} + \tilde{\delta}\frac{\partial^2}{\partial X^2}\right)\omega_z + \tilde{g}_1 \frac{\partial}{\partial Y}\left[A^*\left(\frac{\partial}{\partial X} - i\frac{\partial^2}{\partial Y^2}\right)A + c.c.\right], \tag{24}$$

$$\frac{\partial \omega_z}{\partial Y} = -\left(\frac{\partial^2}{\partial Y^2} + \tilde{\delta}\frac{\partial^2}{\partial X^2}\right)B_x, \tag{25}$$

where the coefficients $\{\tilde{\gamma}_1, \tilde{\delta}$ and $\tilde{g}_1\}$ are calculated as follows: Let $\tilde{f} = f(Q \to 0)$, then these coefficients can be explicitly written in compact form as: $\tilde{\gamma}_1 = \sqrt{3}/(P_r + 1)$, $\tilde{\delta} = \sqrt{3\epsilon}/4$ and $\tilde{g}_1 = 2(P_r + 1)/P_r^2$. The last Eqs. (23)–(25) are similar to those derived by Zippelius and Siggia [14]. Further, in the infinite Prandtl number limit, the contribution of B_x can be neglected and the standard nonlinear two dimensional Landau–Ginzburg equation was recovered and is given as:

$$\frac{\partial A}{\partial T} = A + \left(\frac{\partial}{\partial X} - i\frac{\partial^2}{\partial Y^2}\right)^2 A - |A|^2 A. \tag{26}$$

This equation is similar to that obtained by Newell and Whitehead [34] and by Segel [35] independently; and this equation is called as Newell-Whitehead-Segel (NWS) equation. One of the common solution of the NWS equation is a stationary roll solution and is given by $A(X) = R\exp(i\,k_x X)$, where R and k_x are constants. The stability of this solution was studied by including the mean field contributions. The value of C_z was renormalized as $C_z \to C_z/\lambda_5$.

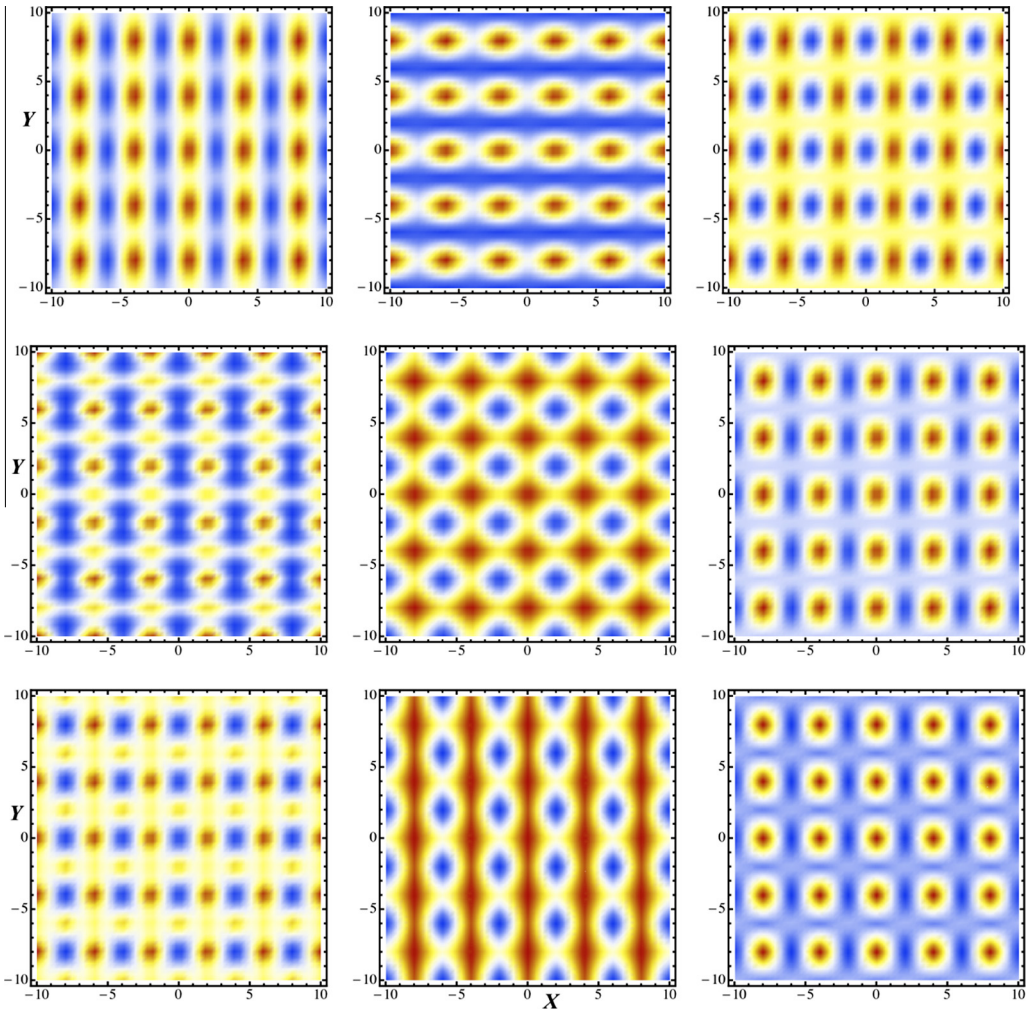

Fig. 4. Density plots of $|A|$ (left), B_x (center) and C_z (right) as a function of both spatial coordinates X and Y at three different times. The fixed parameters are: $P_r = 10$, $P_m = 0.5$ and $Q = 10^2$ and $\epsilon = 0.1$.

4. Patterns selection

In this section, the pattern selection based on the set of amplitude Eqs. (18)–(22) derived in the previous section is developed. In order to understand how a non-optimal pattern wave length can lead to instability, a perfect roll pattern slightly above the critical wavenumber was considered and it is given by

$$A = A^{(s)}(X) = R_0 \exp(iKX), \quad B_x = B_x^{(s)} = 0, \quad C_z = C_z^{(s)} = 0, \tag{27}$$

where R_0 and K are constants. Substituting (27) into Eq. (18), we obtain that $R_0 = \sqrt{1-K^2}$. Since R_0 must to be real, we have imposed a condition that $K^2 < 1$. Therefore, the marginal stability exist when $K = 1$. To examine the pattern stability, small perturbations in the roll amplitude and in the phase are added. Hence, the complex function $A(X,Y,T)$ can be written as:

$$A = R_0(1+u)\exp(i(KX+\phi)), \tag{28}$$

where $u = u(X,Y,T)$, $\phi = \phi(X,Y,T)$ and are chosen such that $|u| \ll 1$ and $|\phi| \ll 1$. Substituting the envelope Eq. (28) in Eq. (18), then linearizing u, B_x, C_z and the gradients of ϕ, the amplitude Eqs. (18)–(22) were reduced to the following equations.

$$\frac{\partial u}{\partial T} = -2(1-K^2)u + \left(\frac{\partial^2}{\partial X^2} + 2K\frac{\partial^2}{\partial Y^2} - \frac{\partial^4}{\partial Y^4}\right)u - 2K\frac{\partial \phi}{\partial X} + 2\frac{\partial^3 \phi}{\partial X \partial Y^2} - C_z, \tag{29}$$

$$\frac{\partial \phi}{\partial T} = \left(\frac{\partial^2}{\partial X^2} + 2K\frac{\partial^2}{\partial Y^2} - \frac{\partial^4}{\partial Y^4}\right)\phi + 2K\frac{\partial u}{\partial X} - 2\frac{\partial^3 u}{\partial X \partial Y^2} - B_x, \tag{30}$$

$$\gamma_1\left(\frac{\partial^2}{\partial Y^2} + \delta\frac{\partial^2}{\partial X^2}\right)\frac{\partial B_x}{\partial T} + \left(\frac{\partial^2}{\partial Y^2} + \delta\frac{\partial^2}{\partial X^2}\right)^2 B_x = 2g_1(1-K^2)\frac{\partial^2}{\partial Y^2}\left(\frac{\partial u}{\partial X} + \frac{\partial^2 \phi}{\partial Y^2}\right), \tag{31}$$

$$\gamma_2\left(\frac{\partial^2}{\partial Y^2} + \delta\frac{\partial^2}{\partial X^2}\right)\frac{\partial C_x}{\partial T} + \left(\frac{\partial^2}{\partial Y^2} + \delta\frac{\partial^2}{\partial X^2}\right)^2 C_z = -2g_2\left(1-K^2\right)\left(\frac{\partial}{\partial X} + \frac{\partial^2}{\partial Y^2}\right)\frac{\partial^2 u}{\partial Y^2} \tag{32}$$

Define the vector field $\mathbf{U}$ as $(u, \phi, B_x, C_x)^T$, that contains the important variables for the linear analysis. Using the standard techniques, the spatial and temporal dependencies of $\mathbf{U}$ are separated by using the normal mode expansion and are given by

$$\mathbf{U}(X,Y,T) = \mathbf{U}_0 \exp[i(q_X X + q_Y Y) + \sigma T] \tag{33}$$

where (q_X, q_Y) are wavenumbers along the (X,Y) directions, respectively; and $\sigma = \sigma_r + i\sigma_i$ denotes the complex eigenvalues in which σ_r is the growth factor of the perturbation, and σ_i its frequency.

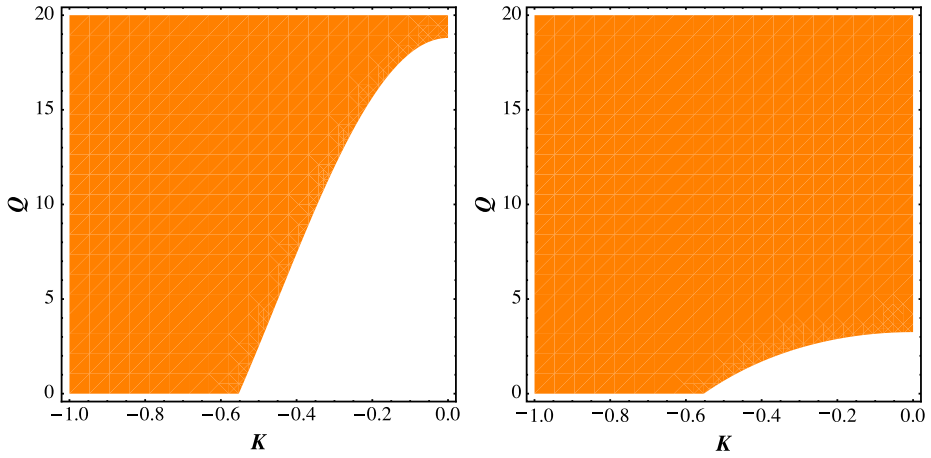

Fig. 5. Existence region of the zig-zag instability as a function of K and Q at $P_m = 0.1$ (left) and $P_m = 0.5$ (right) for $P_r = 10$.

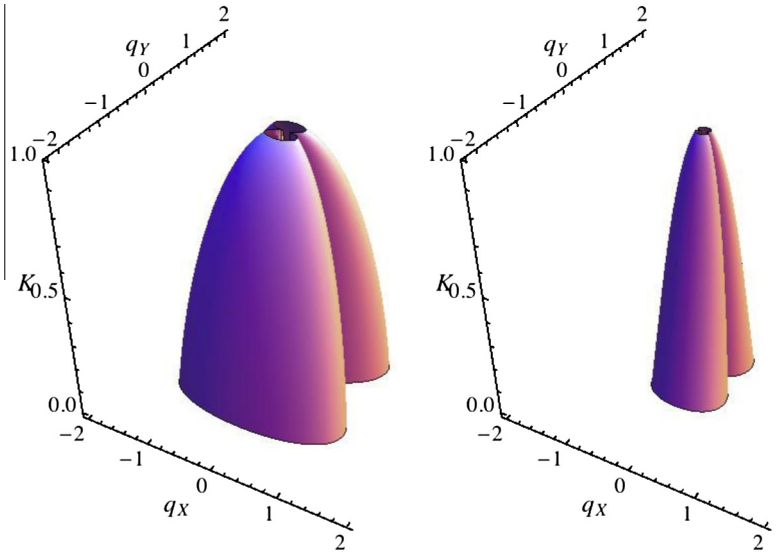

Fig. 6. Instability region as a function of q_x and q_y and K at $P_m = 0.1$ (left) and $P_m = 0.5$ (right) for $P_r = 10$, $Q = 10^2$, and $\epsilon = 0.01$.

In the stationary case ($\sigma = 0$), zig-zag and Eckhaus instabilities were recovered. Apart from these two instabilities, a skew-varicose instability was also obtained and it demands the contribution of mean flow effects.

4.1. Zig-zag instability

The zig-zag instability occurs only along Y-direction i.e., parallel to roll axes. By setting $q_X = 0$ in the normal mode solutions of u and ϕ and using the resultant normal modes in Eqs. (29)–(32), we get

$$2Kq_Y^2 + q_Y^4 + 2g_1(1 - K^2) < 0. \tag{34}$$

The above inequality (34) holds when $K < 0$. Hence, if $K = -q_Y^2$, Eq. (34) gives

$$\frac{K^2}{1 - K^2} > 2g_1. \tag{35}$$

Consequently, the zig-zag instability occurs at the interval

$$K^2 < 1 \quad \text{and} \quad \frac{K^2}{1 - K^2} > 2g_1. \tag{36}$$

Fig. 5 shows the existence of zig-zag instability as a function of roll wavenumber, K and Q for different values of the P_m. From this figure it can be observed that if P_m increases the instability regime requires lower values of Q.

4.2. Eckhaus instability

Eckhaus instability arises from the perturbation that vary only along X-direction, i.e., $q_Y = 0$. Following a similar procedure as in the case of zig-zag instability, the condition $K^2 < 1/3$ is obtained. Therefore, the region for the Eckhaus instability is bounded in region $1/3 < K^2 < 1$. It can be noted that, this condition for the Eckhaus instability has the same form of a simple fluid.

4.3. Skew-varicose instability

After some algebra, one can obtain the general condition for the system's instability and it is given by

$$\xi = \left(2(1-K^2) + \left(q_X^2 + 2Kq_Y^2 + q_Y^4\right)\right)\left(\left(q_X^2 + 2Kq_Y^2 + q_Y^4\right) + \frac{2g_1(1-K^2)q_Y^4}{\left(q_Y^2+q_X^2\delta\right)^2}\right)$$
$$-4q_X^2\left(K + q_Y^2 + \frac{g_1(1-K^2)q_Y^2}{\left(q_Y^2+q_X^2\delta\right)^2}\right)\left(K + q_Y^2 + \frac{g_2(1-K^2)q_Y^2}{q_X\left(q_Y^2+q_X^2\delta\right)}\right) < 0. \tag{37}$$

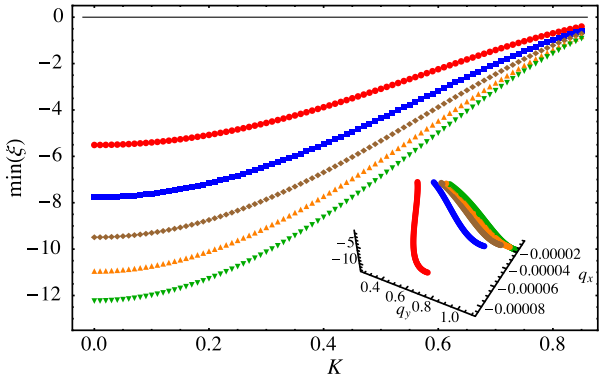

Fig. 7. Minimum value of ξ as a function of K for different values of Q, where {•,■,♦,▲,▼} depict $Q = \{1,2,3,4,5\} \times 10^2$. The inset shows the min (ξ) as a function of q_X and q_Y. The fixed parameters are: $P_r = 10$, $K = 0.5$ and $\epsilon = 0.01$.

Fig. 6 shows the general instability condition as a function of q_X and q_Y for two different values of the P_m. This figure shows that the instability region increases when P_m increases. It can be noticed that when $Q = 0$ and $K = 0$, $\tilde{g}_1 > 3 + 2\sqrt{2}$ or $P_r < P_r^* = 0.78197$. This result is in agreement for instability of rolls calculated by Zipplius and Siggia [14] for the Rayleigh–Benard model in the absence of magnetic field.

Since the relationship (37) cannot be solved analytically, expect for certain limiting cases such as in the case of $q_X = 0$ or of $q_Y = 0$, or in the non-magnetic case ($Q = 0$) when $K = 0$, the most critical modes were calculated numerically. Fig. 7 shows the minimum value of ξ as a function of the wavenumber of the idealized roll, K, for different values of the Q. It is observed that minimum value of ξ is less when K is small. For small values of K and increasing values of Q, ξ value decreases but when K value is close to the unity all ξ values merge to the same value. In addition, $q_X \sim 0$ and $q_Y \sim 1$, when other parameters are fixed. This result implies that the most of the critical modes appear close to the zig-zag instability.

5. Final remarks

In the present work the Rayleigh–Benard convection in an electrically conducting liquid in presence of an applied magnetic field is studied in the case of idealized boundary conditions. The stability threshold for the stationary convection was determined. Close to the bifurcation, the weakly nonlinear stability analysis had been performed in which the mean flow effects were included. In this approach a system of three coupled amplitude equations were derived and their coefficients are analytically calculated. In the limit of large Prandtl number the mean flow effect can be neglected and in this case the standard NWS equation was recovered. Finally the region in which the Eckhaus, zigzag and skew-varicose secondary instabilities occur had been analyzed. The present study will be extended to analyze the oscillatory instabilities and is considered for the future work.

Acknowledgments

We thank to T. Corrales (MPI-P) for his critical reading of the manuscript. D.L. acknowledges the partial financial support from FONDECYT 1120764, Millennium Scientific Initiative, P10-061F, Basal Program Center for Development of Nanoscience and Nanotechnology (CEDENNA) and UTA-project 8750-12.

Appendix A. Derivation of the dimensionless perturbed Eqs. (1)–(5)

The dimensional equations for magnetoconvection under the Boussinesq approximation are [5]:

$$\nabla'.\mathbf{V}' = 0, \tag{A.1}$$

$$\left[\frac{\partial \mathbf{V}'}{\partial t'} + (\mathbf{V}'.\nabla')\mathbf{V}'\right] = -\frac{\nabla' P'}{\rho_0} + \nu\nabla'^2\mathbf{V}' + \frac{\rho}{\rho_0}\mathbf{g} + \frac{\mu_m}{4\pi\rho_0}(\nabla'\times\mathbf{H}')\times\mathbf{H}', \tag{A.2}$$

$$\frac{\partial \tau'}{\partial t'} + (\mathbf{V}'.\nabla')\tau' = \kappa\nabla'^2\tau', \tag{A.3}$$

$$\frac{\partial \mathbf{H}'}{\partial t'} = \nabla'\times(\mathbf{V}'\times\mathbf{H}') + \eta\nabla'^2\mathbf{H}', \tag{A.4}$$

$$\nabla'.\mathbf{H}' = 0. \tag{A.5}$$

where $(\nabla'\times\mathbf{H}')\times\mathbf{H}' = -\frac{1}{2}\nabla'|\mathbf{H}'|^2 + (\mathbf{H}'.\nabla')\mathbf{H}', \mathbf{H}' = H_0'\hat{\mathbf{z}} + \left(H_x'\hat{\mathbf{x}} + H_y'\hat{\mathbf{y}} + H_z'\hat{\mathbf{z}}\right)$ and the density $\rho = \rho_0[1 - \alpha(\tau' - \tau_0')]$ is considered to be independent of pressure (i.e., incompressibility is assumed) and depends linearly on temperature.

Now we obtain Eq. (2) in the following manner. Thus, equation (A.2) is simplified to

$$\left[\frac{\partial \mathbf{V}'}{\partial t'} + (\mathbf{V}'.\nabla')\mathbf{V}'\right] = -\nabla'\left(\frac{P'}{\rho_0} + \frac{\mu_m}{8\pi\rho_0}|\mathbf{H}'|^2\right) + \nu\nabla'^2\mathbf{V}' + \frac{\rho}{\rho_0}\mathbf{g} + \frac{\mu_m}{4\pi\rho_0}(\mathbf{H}'.\nabla')\mathbf{H}', \tag{A.6}$$

The conduction state is characterized by

$$\mathbf{V}_s' = 0, \tau_s' = \tau_0' - \left(\frac{\Delta\tau'}{d}\right)z',$$
$$P_s' = P_0 - g\rho_0\left(z' + \frac{1}{2}\alpha\beta z'^2\right), \quad \text{and} \quad \mathbf{H}_s' = H_0'\hat{\mathbf{z}}, \tag{A.7}$$

where suffix 's' stands for the static state, $\beta = \Delta\,\tau'/d$ and H_0' represents the externally imposed vertical magnetic field.

To study the onset of convection the small perturbations are introduced in the conduction state solutions as $\mathbf{V}' = \mathbf{V}_s' + \mathbf{V}_*'$, $\tau' = \tau_s' + \theta_*'$, $P' = P_s' + P_*'$ and $\mathbf{H}' = \mathbf{H}_s' + \mathbf{H}_*'$, where $\mathbf{V}_*', \theta_*', P_*', \mathbf{H}_*'$ represent the perturbed quantities. Thus, the last term of equation (A.2) in right hand side (RHS) is modified as

$$\frac{\mu_m}{4\pi\rho_0}(\mathbf{H}'.\nabla')\mathbf{H}' = \frac{\mu_m}{4\pi\rho_0}\left((\mathbf{H}_s' + \mathbf{H}_*').\nabla'\right)\left(\mathbf{H}_s' + \mathbf{H}_*'\right). \tag{A.8}$$

Using the conduction state solution $\mathbf{H}_s' = H_0'\hat{\mathbf{z}}$, which is given by equation (A.7), the above equation (A.8) reduces to

$$\frac{\mu_m}{4\pi\rho_0}(\mathbf{H}'.\nabla')\mathbf{H}' = \frac{\mu_m}{4\pi\rho_0}\left[(\mathbf{H}_s'.\nabla')\mathbf{H}_*' + (\mathbf{H}_*'.\nabla')\mathbf{H}_*'\right] \tag{A.9}$$

(or)

$$\frac{\mu_m}{4\pi\rho_0}(\mathbf{H}'.\nabla')\mathbf{H}' = \frac{\mu_m H_0'}{4\pi\rho_0}\frac{\partial \mathbf{H}_*'}{\partial z'} + \frac{\mu_m}{4\pi\rho_0}(\mathbf{H}_*'.\nabla')\mathbf{H}_*'. \tag{A.10}$$

Applying the similar analysis to the other terms of equation (A.2), the dimensional perturbed momentum equation along with the Lorentz force for the magnetoconvection model under the Boussinesq approximation is given by:

$$\left[\frac{\partial \mathbf{V}_*'}{\partial t'} + (\mathbf{V}_*'.\nabla')\mathbf{V}_*'\right] = -\nabla'\left(\frac{P'}{\rho_0} + \frac{\mu_m}{8\pi\rho_0}|\mathbf{H}_*'|^2\right) + \nu\nabla'^2\mathbf{V}_*' + \frac{\rho}{\rho_0}\mathbf{g} + \frac{\mu_m H_0'}{4\pi\rho_0}\frac{\partial \mathbf{H}_*'}{\partial z'} + \frac{\mu_m}{4\pi\rho_0}(\mathbf{H}_*'.\nabla')\mathbf{H}_*'. \tag{A.11}$$

We have used a Cartesian system of coordinates whose dimensionless vertical coordinate z' and horizontal coordinates x', y' are scaled based on depth of the layer, d. The quantities $\mathbf{V}_*', \theta_*', t', P_*'$ and $\mathbf{H}_*'$ are made dimensionless by scales $\kappa/d, \Delta\tau', d^2/\kappa, \rho_0\kappa^2/d^2$ and $\kappa H_0'/\eta$, respectively.

Using the above scaling, the perturbed basic dimensional governing momentum equation (A.11), in non-dimensional form is given by:

$$\frac{1}{P_r}\left[\frac{\partial \mathbf{V}}{\partial t}+(\mathbf{V}.\nabla)\mathbf{V}\right]-\frac{QP_m}{P_r}(\mathbf{H}.\nabla)\mathbf{H} = -\nabla\left(\frac{P}{P_r}+\frac{Q}{2}\frac{P_m}{P_r}|\mathbf{H}|^2+QH_z\right)+\nabla^2\mathbf{V}+Ra\theta\hat{\mathbf{z}}+Q\frac{\partial \mathbf{H}}{\partial z} \tag{A.12}$$

(or)

$$\frac{1}{P_r}d_t\mathbf{V}-\frac{QP_m}{P_r}(\mathbf{H}.\nabla)\mathbf{H} = -\nabla p_{eff}+\nabla^2\mathbf{V}+Q\frac{\partial \mathbf{H}}{\partial z}+Ra\theta\hat{\mathbf{z}}. \tag{A.13}$$

It can be noted that in equation (A.12) or equation (A.13), for convenient, we have omitted the asterisk.

By following the above procedure, the perturbed non-dimensional Eqs. (1), (3), (4) and (5) can be derived from the equations (A.1), (A.3), (A.4) and (A.5) respectively.

Appendix B. Coefficients

The coefficients λ_j which appear in the amplitude Eqs. (18)–(22) are given by:

$$\lambda_0 = \pi^2 Q\zeta_{sc}^2+\zeta_{sc}^6\left(1+\frac{1+P_m}{P_r}\right)-\frac{k_{sc}^2P_mRa_{sc}}{P_r}, \tag{38}$$

$$\lambda_1 = k_{sc}^2\left(6\zeta_{sc}^4+\pi^2Q-Ra_{sc}\right), \tag{39}$$

$$\lambda_2 = k_{sc}^2\zeta_c^2Ra_{sc}, \tag{40}$$

$$\lambda_3 = -\frac{\pi^4Q}{2}\left(\frac{P_m}{P_rk_{sc}}\right)^2\left(\pi^2-k_{sc}^2\right)+\frac{k_{sc}^2Ra_{sc}}{2}, \tag{41}$$

$$\lambda_4 = k_{sc}^2Ra_{sc}+\frac{\zeta_{sc}^2}{P_r}\left(\zeta_{sc}^4-\pi^2QP_m\right), \tag{42}$$

$$\lambda_5 = \frac{2\pi^2QP_m\zeta_{sc}^4}{P_r}, \tag{43}$$

$$\lambda_6 = \frac{QP_m}{Ra_{sc}}\left(\zeta_{sc}^2-\frac{\pi^4Ra_{sc}}{2k_{sc}^2\zeta_{sc}^2}\right)+\frac{\zeta_{sc}^4}{\zeta_{sc}^4+\pi^2Q}, \tag{44}$$

$$\lambda_7 = \frac{\pi^2}{k_{sc}^2\zeta_{sc}^2}. \tag{45}$$

References

[1] M. Schussler, A. Vogler, Magnetoconvection in a sunspot umbra, Astrophys. J. 64 (2006) L73–L76.
[2] J.H. Thomas, N.O. Weiss (Eds.), Sunspots: Theory and Observations, NATO ASI Series C375, 3, 1992.
[3] D.W. Hughes, M.R.E. Proctor, Magnetic-fields in the solar convection zone - magnetoconvection and magnetic buoyancy, Annu. Rev. Fluid Mech. 20 (1988) 187–223.
[4] D.J. Galloway, N.O. Weiss, Convection and magnetic-fields in stars, Astrophys. J. 243 (1981) 945–953.
[5] S. Chandrasekhar, Hydrodynamic and Hydromagnetic Stability, Oxford University Press, 1961.
[6] M.R.E. Proctor, N.O. Weiss, Magnetoconvection, Rep. Prog. Phys. 45 (1982) 1317–1379.
[7] Y. Nakagawa, Experiments on the stability of a layer of mercury heated from below and subjects to the simultaneous action of a magnetic field and rotation, Proc. R. Soc. Lond. A242 (1957) 81–88.
[8] F.H. Busse, A model of the geodynamo, Geophys. J.R. Astr. Soc. 42 (1957) 437–459.
[9] N.O. Weiss, Convection in an imposed magnetic field. Part 1: The development of nonlinear convection, J. Fluid Mech. 108 (1981) 247–272.
[10] N.O. Weiss, Convection in an imposed magnetic field. Part 2: The dynamical regime, J. Fluid Mech. 108 (1981) 273–289.
[11] F.H. Busse, R.M. Clever, On the stability of convection rolls in the presence of a vertical magnetic field, Phys. Fluids 25 (1982) 931–935.
[12] R.M. Clever, F.H. Busse, Nonlinear oscillatory convection in the presence of a vertical magnetic field, J. Fluid Mech. 201 (1989) 507–523.
[13] A. Zippelius, E.D. Siggia, Disappearance of stable convection between free-slip boundaries, Phys. Rev. A. 26 (1982) 1788–1790.
[14] A. Zippelius, E.D. Siggia, Stability of finite-amplitude convection, Phys. Fluids 26 (1983) 2905–2915.
[15] F.H. Busse, E.W. Bolton, Instabilities of convection rolls with stress-free boundaries near threshold, J. Fluid Mech. 146 (1984) 115–125.
[16] A.J. Bernoff, Finite amplitude convection between stress-free boundaries: Ginzburg–Landau equations and modulation theory, Eur. J. Appl. Math 5 (1994) 267–282.
[17] A. Mielke, Mathematical analysis of sideband instabilities with application to Rayleigh–Benard convection, J. Nonlinear Sci. 7 (1997) 57–99.
[18] O.M. Podvigina, On stability of rolls near the onset of convection in a layer with stress-free horizontal boundaries, Geophys. Astrophys. Fluid Dyn. 104 (2010) 1–28.
[19] S.M. Cox, P.C. Matthews, Instability of rotating convection, J. Fluid Mech. 403 (2000) 153–172.
[20] A.A. Golovin, A.A. Nepomnyashchy, L.M. Pismen, Interaction between short scale Marangoni convection and long scale deformational bifurcation, Phys. Fluid 6 (1994) 34–48.
[21] P.C. Matthews, S.M. Cox, Pattern formation with Galilean invariance, Phys. Rev. E 62 (2000) R1473–R1476.
[22] P.C. Matthews, S.M. Cox, Pattern formation with conservation law, Nonlinearity 13 (2000) 1293–1320.
[23] S.M. Cox, P.C. Matthews, New instabilities in two-dimensional rotating convection and magnetoconvection, Physica D 149 (2001) 210–229.
[24] E. Knobloch, N.O. Weiss, L.N. Dacosta, Oscillatory and steady convection in a magnetic-field, J. Fluid Mech. 113 (1981) 153–186.
[25] E. Knobloch, N.O. Weiss, Bifurcations in a model of magnetoconvection, Physica D 9 (1983) 379–407.
[26] T. Clune, E. Knobloch, Pattern selection in 3-dimensional magnetoconvection, Physica D 74 (1994) 151–176.
[27] S. Blanchflower, N. Weiss, Three-dimensional magnetohydrodynamic convections, Phys. Lett. A 294 (2002) 297–303.
[28] S.M. Cox, P.C. Matthews, S.L. Pollicott, Swift–Hohenberg model for magnetoconvection, Phys. Rev. E 69 (2004) 066314. and reference therein.
[29] J.H.P. Dawes, Localized convection cells in the presence of a vertical magnetic field, J. Fluid Mech. 570 (2007) 385–406.
[30] D. Lo Jacono, A. Bergeon, E. Knobloch, Magnetohydrodynamic convections, J. Fluid Mech. 687 (2011) 595–605.
[31] F.M. White, Viscous Fluid Flow, third ed., McGraw-Hil, New York, 2006.
[32] Y.S. Lee, C.H. Chun, Experiments on the oscillatory convection of low Prandtl number liquid in Czochralski configuration for crystal growth with cusp magnetic field, J. Cryst. Growth 180 (1997) 477–486.
[33] A.A. Schekochihin, S.A. Boldyrev, R.M. Kulsru, Spectra and growth rates of fluctuating magnetic fields in the kinematic dynamo theory with large magnetic Prandtl numbers, Astrophys. J. 567 (2002) 828–852.
[34] A.C. Newell, J.A. Whitehead, Finite bandwidth,finite amplitude convection, J. Fluid Mech. 38 (1969) 279–303.
[35] L.A. Segel, Distant side-walls cause slow amplitude modulation of cellular convection, J. Fluid Mech. 38 (1969) 203224.